IGA of a Photocathode

1 60 kV Geometry

1.1 Geometry

The 60 kV geometry was derived from the technical drawings in [1]. Some simplifications were made especially regarding the inner part of the electrode, such that the geometry may be modeled as being rotationally symmetric. The dimensions of the electrode, puck, puck elevator, vacuum chamber and insulator were derived from Figure A.1, A.2, A.3, A.4 and A.6 in [1] respectively. The geometry of the vacuum chamber was also simplified to reduce the computational domain and the reduced insulator geometry is in part based on the drawing in Figure 5.7 of the thesis. The boundary conditions were retrieved from Table 5.1 in [1] and the relative permittivity of the insulator was taken from an existing CST model to be 9.4.

The geometry is depicted in fig. 1 and a technical drawing of the actual geometry is given in fig. 2 for comparison. The numbers in the simplified geometry refer to the individual patches in the context of IGA. The patch boundaries are indicated by the black lines. The red lines represent homogeneous Dirichlet boundary conditions, the blue lines inhomogeneous Dirichlet boundary conditions with a value of -60 kV and the green lines indicate homogeneous Neumann boundaries. According to the technical drawings patch 10 as well as parts of patches 7 and 8 are modeled as insulator material.

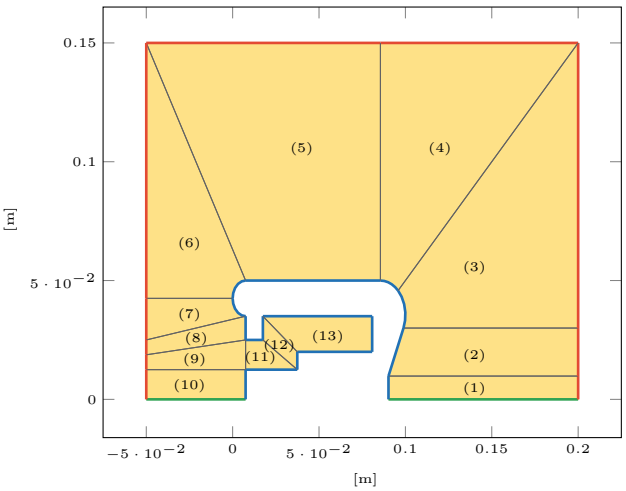

Figure 1: 60 kV Photocathode geometry and boundary conditions.

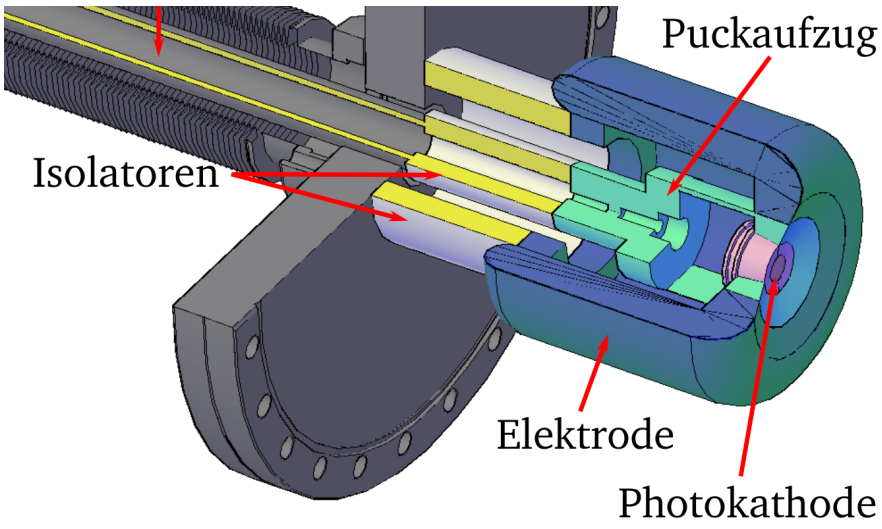

Figure 2: Part of the CAD drawing of the geometry.

1.2 Electrostatic Potential and Electric Field

The solution for the electrostatic potential is shown in fig. 3. Fig. 4 depicts the absolute value of the electric field. Both of the solutions were computed with $p = 4$ as the degree of the basis functions and $n_{\text{sub}} = 128$ as the number of elements that each knot vector is uniformly split into. To give a comparison with the previous simulations fig. 5 shows the results depicted in the thesis [1]. It is visible that the solutions are similar with the peak values appearing near the circular parts of the electrode. However the new results indicate that the absolute largest values occur at the back of the electrode and they also show higher field magnitudes in the insulator regions. This is a clear contrast to the previous simulation. A second comparison can be made with the updated CST model from fig. 6 from [2]. The absolute largest field values appear in the same region, however their magnitude is higher. The bevavior of the field at the triple point is also very similar in that the surrounding magnitudes are very small.

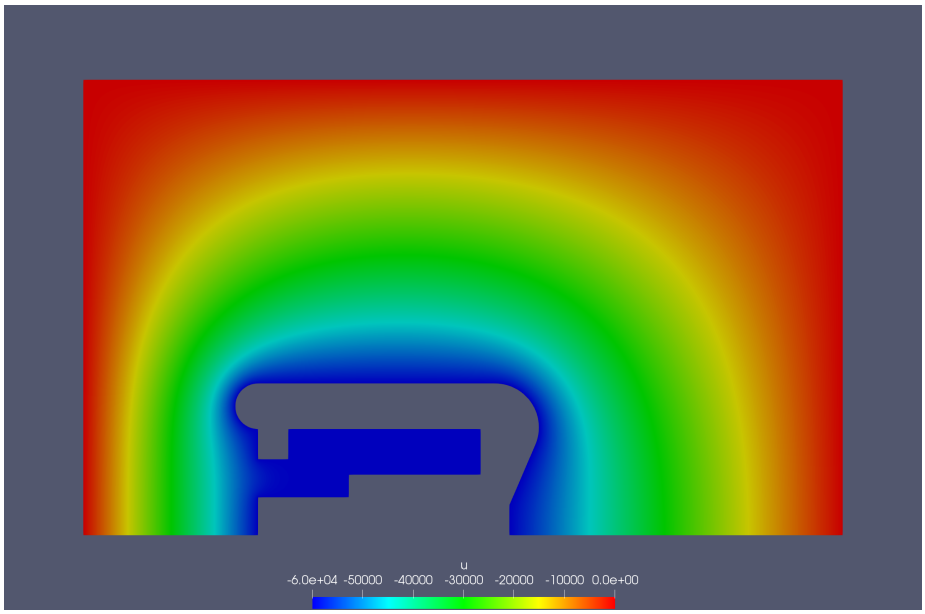

Figure 3: Electrostatic potential.

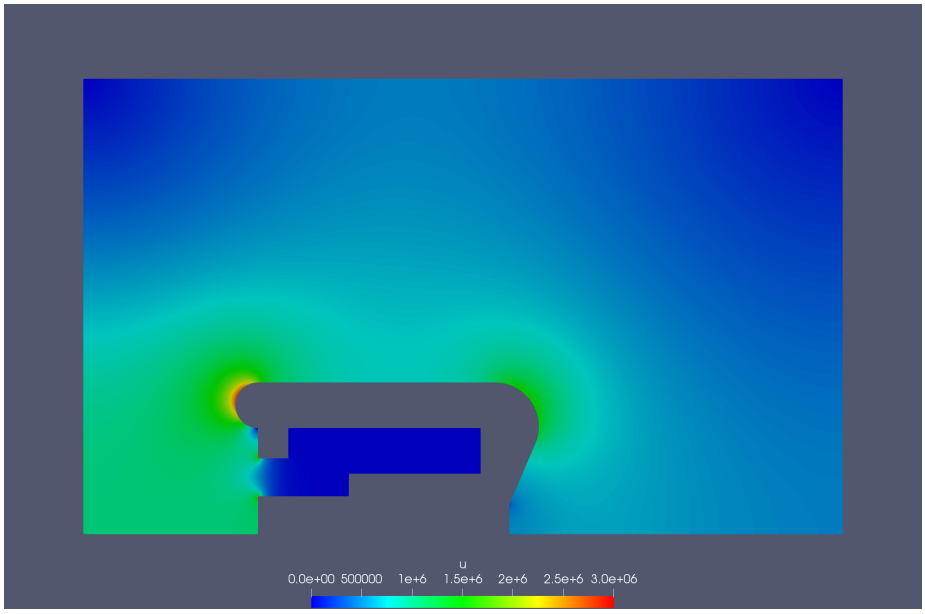

Figure 4: Absolute value of the electric field.

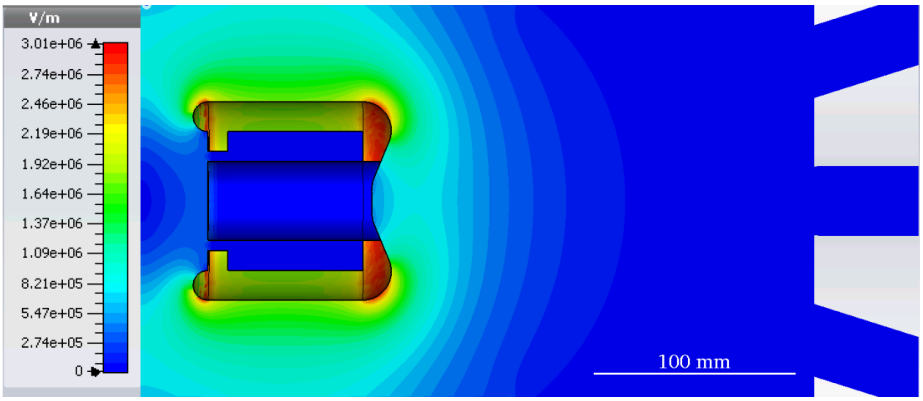

Figure 5: Results from the PhD thesis.

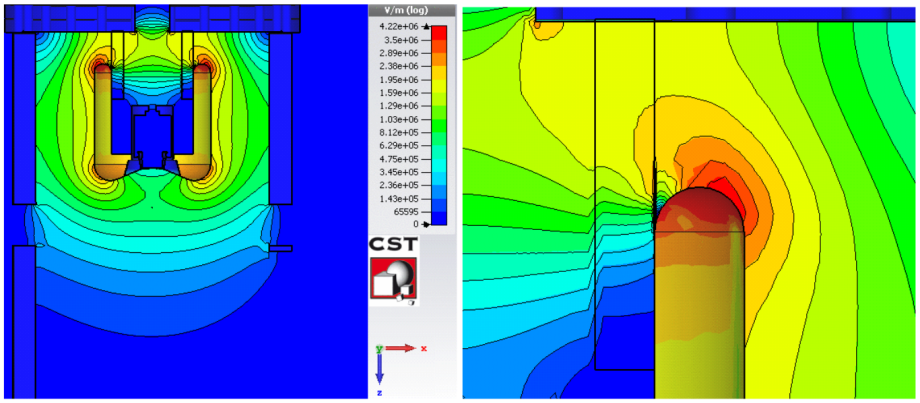

Figure 6: Results from the Bachelor thesis.

1.3 Convergence Study

The convergence studies investigate the accuracy of the solution while increasing the number of elements per patch. (Akin to h-refinement in classical FEA) Since no analytic solution exists we used a reference with $n_{\text{sub}} = 256$ and $p = 4$ as a comparison. The errors are computed as

$$e_{L^2} = \frac{\|\varphi_{\text{it}} - \varphi_{\text{ref}}\|_{L^2}}{\|\varphi_{\text{ref}}\|_{L^2}} \tag{1}$$

$$e_{H^1} = \frac{\|\varphi_{\text{it}} - \varphi_{\text{ref}}\|_{H^1}}{\|\varphi_{\text{ref}}\|_{H^1}} \tag{2}$$

where

$$\|\varphi\|_{H^1} = \sqrt{\|\varphi\|_{L^2}^2 + \|\nabla\varphi\|_{L^2}^2}. \tag{3}$$

Here φ denotes the electrostatic potential. The integrals associated with the L^2-norm are evaluated using a quadrature rule defined on each element of a given patch.

The degrees of the basis functions are given in the legend, as well as theoretical limits for the convergence rates. They are given by $p+1$ in the case of the L^2-norm (electrostatic potential) and p in the case of the H^1-norm (electric field). As seen in fig. 7 and fig. 8 we observe convergence, however the convergence rate appears to be limited.

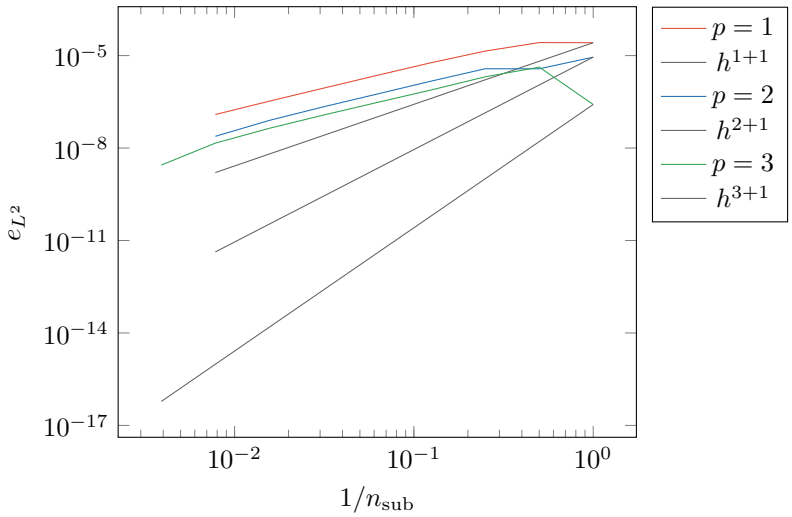

Figure 7: Convergence of L^2-norm.

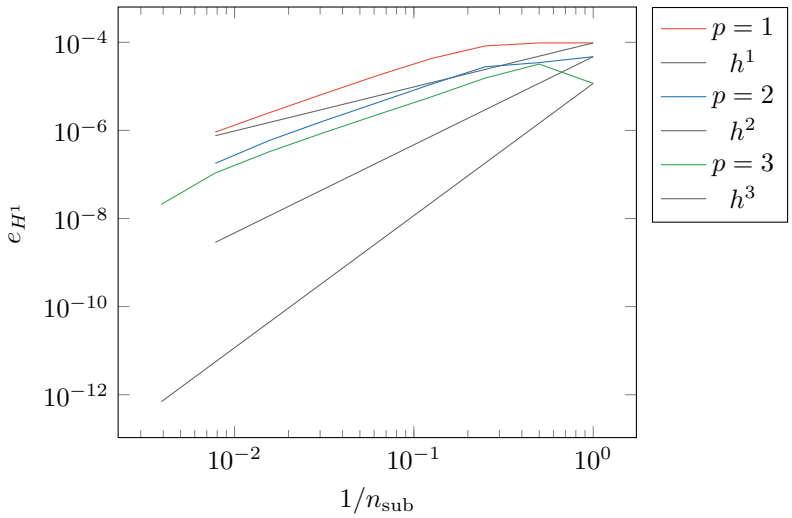

Figure 8: Convergence of H^1-norm.

Lastly the error in specific regions of the geometry was investigated by displaying the absolute error of the eletric field on every individual element of the mesh. In the case of fig. 9 we chose $n_{\text{sub}} = 256$ and $p = 3$ for the iterative solution and computed the errors with respect to a reference using $n_{\text{sub}} = 256$ and $p = 4$. The figure shows the absolute error on each element in a logarithmic scale. We observe that the errors are largest near sharp corners or large changes in the sizes of the mesh's elements. This is to be expected and as indicated by the colorbar the largest absolute errors come out to be around 19 V/m with the associated field magnitudes being almost exclusively larger than 10 MV/m.

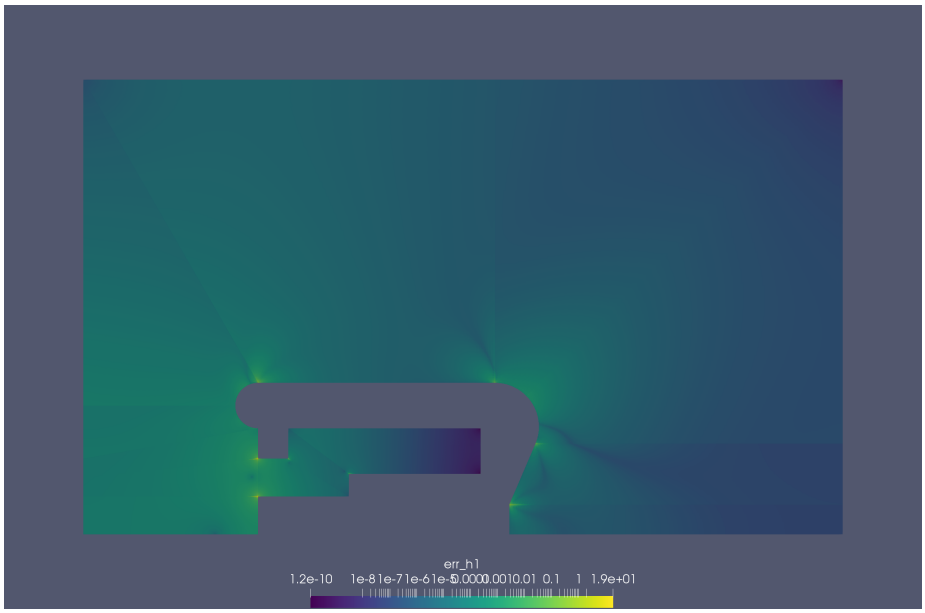

Figure 9: Absolute error of the electric field on every element.

2 200 kV Geometry

2.1 Geometry

The 200 kV geometry was derived from version one of the CST model. Some simplifications were made such that the geometry may be considered rotationally symmetric. The dimensions of the electrode, puck, puck elevator, vacuum chamber and insulator were derived from the model as depicted in fig. 10. The boundary conditions remained the same, except for the increase in voltage, when compared to the 60 kV variant and the relative permittivity of the insulator was taken from the model to be 9.4.

The geometry is depicted in fig. 11. The numbers refer to the individual patches in the context of IGA. The patch boundaries are indicated by grey lines. The red lines represent homogeneous Dirichlet boundary conditions, the blue lines inhomogeneous Dirichlet boundary conditions with a value of -200 kV

and the black lines indicate homogeneous Neumann boundaries. The patches containing insulator material are colored in red.

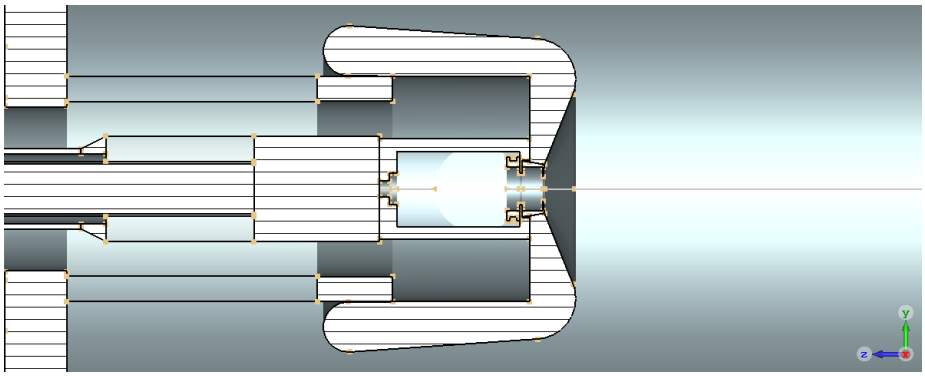

Figure 10: y-z view of the CST model for $x = 0$.

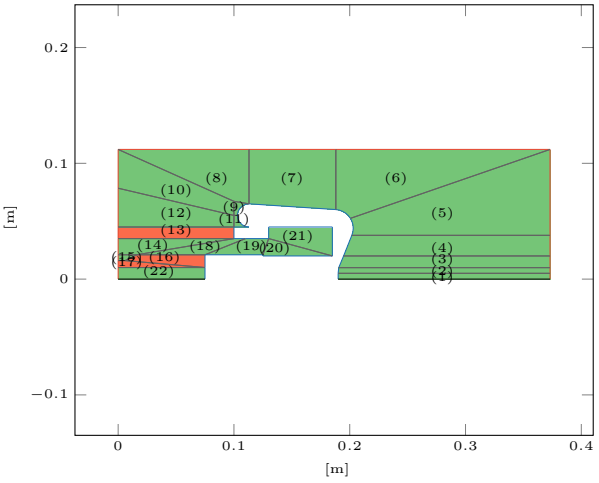

Figure 11: 200 kV Photocathode geometry and boundary conditions.

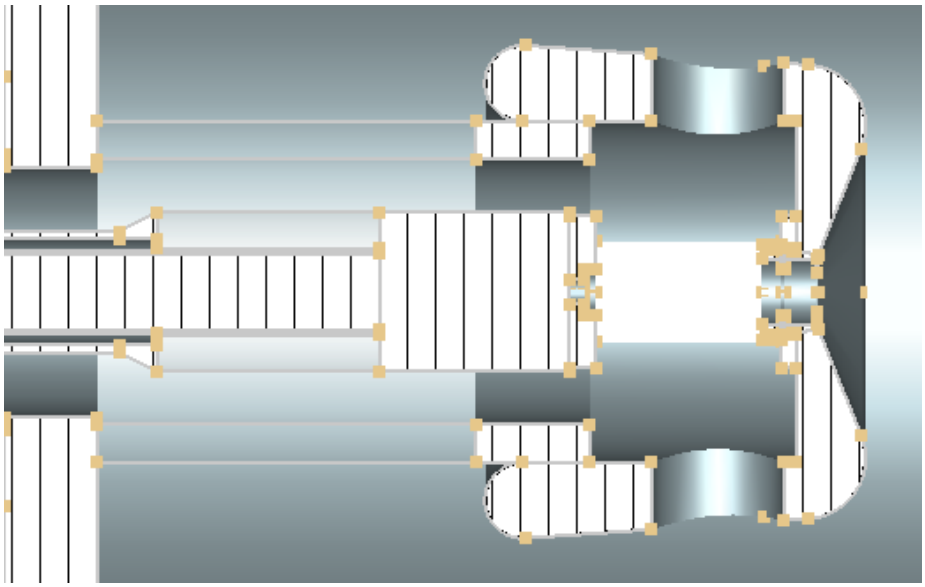

Figure 12: x-z view of the CST model for $y = 0$.

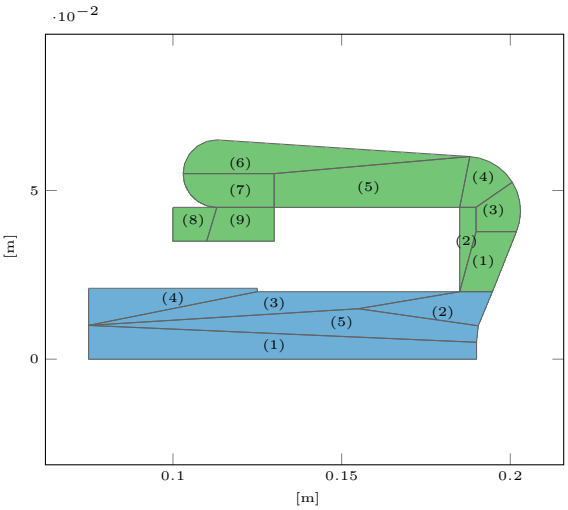

Figure 13: Geometry of the electrode and puck lift.

One of the constraints for the later optimization will be the weight of the electrode and thus its volume. Since we consider the geometry to be rotationally symmetric it suffices to compute the surface of the electrode patches using numerical quadrature. For this purpose the inside of the geometry was discretised as two seperate multipatch domains. The outer part models nearly all of the electrode, however it does not properly take into account the two holes

that can be seen in fig. 12. Furthermore the puck lift was not modeled with great accuracy thus we still need to find a way to properly estimate the entire volume of the electrode. The two multipatch geometries are displayed together in fig. 13 with the electrode patches colored in green and the lift patches colored in blue. The surface area of the electrode comes out to be $A_e = 2305.8\ \text{mm}^2$ and the area of the lift is $A_l = 2377.5\ \text{mm}^2$. The weight of the entire construction follows as $m = 2\pi(A_e + A_l)\rho$ with $\rho = 7.99\frac{\text{g}}{\text{mm}^3}$. (This is clearly wrong, how do I correctly compute the volume? The correct way should be $\int_0^{2\pi} A(r)r\ d\varphi$, but how would I go about this approach since r is not constant?)

2.2 Electrostatic Potential and Electric Field

The solution for the electrostatic potential is shown in fig. 14. Fig. 15 depicts the absolute value of the electric field. Both of the solutions were computed with $p = 4$ as the degree of the basis functions and $n_{\text{sub}} = 128$ as the number of elements that each knot vector is uniformly split into. It is evident that there exist parts of the domain where the magnitude exceeds the limit of $10\frac{\text{MV}}{\text{m}}$. There are also very high gradients visible at the triple points however these also coincide with sharp corners so numerical issues might play a role. (Again perform a convergence study and investigate the absolute error per patch?)

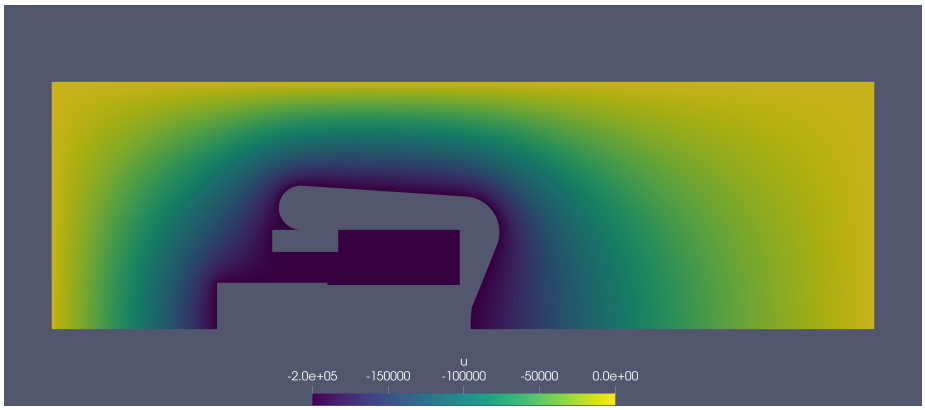

Figure 14: Electrostatic potential.

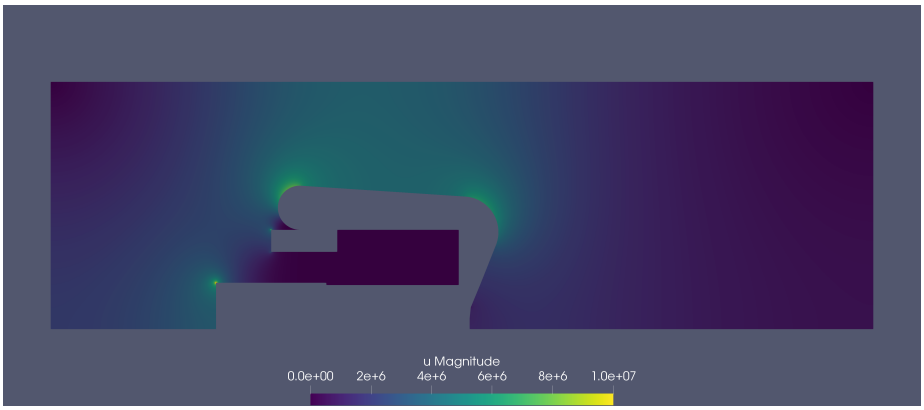

Figure 15: Absolute value of the electric field.

2.3 Optimization

The aim of the optimization will be to minimize the maximal field amplitudes. For practicality we will only look at the critical points of the geometry, i. e. the curvatures of the outer electrode and the triple points and average the field strengths over a given number of sample points. The lower part of the geometry will remain fixed so only the electrode boundaries of patches 5, 6, 7, 8, 9 and 11 from fig. 11 and their respective control points will be the DoFs. Another thing that might be considered is varying the length of the entire electrode. Aside from the fixed part of the geometry we also need to consider the volume constraint as stated previously.

2.4 Astra

In the future we may also optimize the electrode boundary next to the puck, i. e. patches 2, 3 and 4 to obtain optimal particle trajectories. The cost function will be computed using Astra. (Perform all the tests for Astra also for the final Photocathode geometry?) The desired total bunch charge is 10 pC with a beam current of $(20 - 100)$ μA, whereas a typical value would be 100 fC. The bunch length is around 5 ps with a normalized transversal emittance of $e_{x,y} \leq 1$ mm mrad. The desired energy resolution is $\frac{\Delta E}{E} \leq 10^{-4}$. The tracking will be performed using individual bunches from a pulsed laser. The emission model may be derived from [3].

References

[1] Martin Espig. *Development, construction and characterization of a variable repetitive spin-polarized electron gun with an inverted-geometry insulator.* PhD thesis, Technische Universität Darmstadt, 2016.

[2] Vincent Wende. Simulations for investigation and improvements on a spin-polarized electron source with inverted-geometry insulator for the s-dalinac. Master's thesis, Technische Universität Darmstadt, 2017.

[3] Markus Wagner. *Production and investigation of pulsed electron beams at the S-DALINAC.* PhD thesis, Technische Universität Darmstadt, 2013.